Weak shock reflection

By JOHN K. HUNTER[1] AND MOYSEY BRIO[2]

[1]Department of Mathematics and Institute of Theoretical Dynamics, University of California, Davis, CA 95616, USA

[2]Department of Mathematics, University of Arizona, Tucson, AZ 85721, USA

We present numerical solutions of a two-dimensional inviscid Burgers equation which provides an asymptotic description of the Mach reflection of weak shocks. In our numerical solutions, the incident, reflected, and Mach shocks meet at a triple point, and there is a supersonic patch behind the triple point, as proposed by Guderley for steady weak-shock reflection. A theoretical analysis indicates that there is an expansion fan at the triple point, in addition to the three shocks. The supersonic patch is extremely small, and this work is the first time it has been resolved.

1. Introduction

From the beginning, there have been discrepancies between theoretical predictions of weak shock reflection (von Neumann 1963) and experimental observations. In particular, an irregular weak shock reflection closely resembles a single Mach reflection that contains a triple point. The theoretical analysis, however, shows that a standard triple-point configuration, in which three plane shocks and a plane contact discontinuity separated by constant states meet at a point, is impossible for sufficiently weak shocks (Bleakney & Taub 1949; Henderson 1987).

A number of ways to resolve this apparent 'triple-point paradox' have been suggested over the last fifty years: there could be an additional, unobserved wave at the triple point, such as an expansion fan (Bleakney & Taub 1949; Courant & Friedrichs 1976; Guderley 1962; Sternberg 1959), or a fourth shock (Henderson 1966); there could be a singularity in the solution behind the triple point (Richtmeyer 1981; Tabak & Rosales 1994), or a singularity in the reflected shock curvature at the triple point (Sternberg 1959), so that a local approximation of the solution by plane waves separated by constant states is invalid; or the reflected shock could spread out into a continuous wave before hitting the incident shock so that there is, in fact, no triple point (Colella & Henderson 1990; Henderson 1987). A local analysis of the solution near the triple point cannot determine which of these, or other, conceivable structures actually occurs, and a global solution of the problem is required.

An asymptotic problem that describes the Mach reflection of weak shocks off thin wedges was formulated in Hunter (1991). In this problem, the compressible Euler equations are replaced by a two-dimensional generalization of the inviscid Burgers equation, the unsteady transonic small disturbance equation. The asymptotic equations are much simpler to analyse than the full Euler equations, and fewer computational resources are required to solve them numerically.

In this paper, we present numerical solutions of the asymptotic shock reflection problem on an extremely fine grid. As shown in figure 5(*a*), there is a tiny supersonic patch behind the triple point. An independent check on the validity of the asymptotic

solutions is provided by subsequent numerical solutions of the full Euler equations for weak shock reflection off a wall (Brio *et al.* 2000). The full Euler solutions contain a supersonic patch and are remarkably similar to the asymptotic solutions shown here.

The incident shock and a reflected shock of small but non-zero strength collide at the supersonic triple point to form the Mach shock. All three shocks belong to the same family. The waves produced by the collision of the incident and reflected shocks may be determined theoretically by the solution of a local Riemann problem. In addition to the Mach shock, the solution contains an expansion fan in the opposite family to the shocks, thus explaining the apparent 'triple-point paradox'. A schematic diagram of the local structure of the solution near the triple point, inferred from the numerical solution and various theoretical considerations, is shown in figure 9. Guderley (1962) (figure 60, p. 148) proposed essentially the same structure for weak shock reflection in steady transonic flows.

A supersonic patch has never been observed in experiments, but this is not surprising given its extremely small size. For example, suppose that a shock of Mach number 1.04 hits an 11.5° angle wedge. Using our numerical solution of the asymptotic equations to estimate the size of the patch, we find that after the shock has propagated a distance of 1 m along the wedge, the Mach shock height is 0.1 m, the height of the supersonic patch normal to the wedge is 1 mm, and the width of the patch along the wedge is 0.1 mm. We hope that this estimate of the size of the supersonic patch, and the identification of the parameter regime in which it is most easily detected, will enable its experimental observation.

In addition to its physical importance, the shock reflection problem is one of the simplest two-dimensional Riemann problems for hyperbolic systems of conservation laws. These problems are poorly understood from a theoretical point of view because of the difficulty of analysing nonlinear, mixed-type equations whose solutions contain shocks. The presence of a supersonic patch, an embedded sonic line, and a transonic coupling between the solution in the elliptic and hyperbolic regions, seen here, are likely to be typical features of solutions of general two-dimensional Riemann problems. For example, a supersonic patch and the generation of an expansion fan at a shock intersection point appear to occur in the numerical solutions of anomalous shock refraction shown in figure 3 of Puckett, Henderson & Colella (1995).

We now outline the contents of the paper. In §2, we summarize the asymptotic equations for weak shock reflection. In §3, we present our numerical solutions. In §4, we give a theoretical discussion of these solutions, and in §5, we describe the numerical scheme. The asymptotic shock reflection problem is derived in §§6–9. In §6, we formulate the full Euler problem for shock reflection. In §7, we write out the exact solution of the linearized shock reflection problem and describe the regions of the flow where this linearized solution is not uniformly valid. In §8, we summarize the weakly nonlinear expansion valid near the reflection point that leads to the two-dimensional Burgers equation. In §9, we obtain the initial data for the two-dimensional Burgers equation by matching the weakly nonlinear solution with the linearized solution.

2. The asymptotic shock reflection problem

There are two main parameters in the shock reflection problem,

$$M = \text{Mach number of the incident shock,}$$
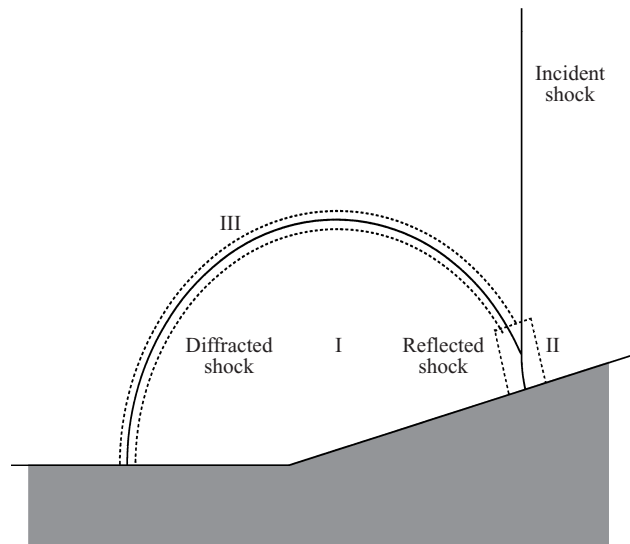$$\theta_w = \text{wedge angle.}$$

FIGURE 1. Regions for the asymptotic solution of weak shock reflection off a thin wedge. The two-dimensional Burgers equation describes the solution in the reflection region II.

Lighthill (1949) studied the reflection of a strong shock by a thin wedge, when

$$\theta_w \to 0, \quad \text{with } M > 1 \text{ fixed.} \tag{2.1}$$

In this limit, Mach reflection always occurs. Lighthill's analysis leads to linearized equations behind the incident shock, and it does not provide a detailed description of the solution near the triple point, where nonlinear effects play a crucial role. For additional work on shock reflection by thin wedges, see Sakurai (1964) and Ting & Ludloff (1952).

Keller & Blank (1951) and Hunter & Keller (1984) studied the reflection of a weak shock by a thick wedge, when

$$M \to 1, \quad \text{with } \theta_w > 0 \text{ fixed.} \tag{2.2}$$

In this limit, regular reflection always occurs. Neither of the limits (2.1) or (2.2) captures the transition from regular to Mach reflection.

The transition from regular to Mach reflection for weak shocks occurs for thin wedges when the shock strength and the wedge angle are related by

$$M - 1 = O(\theta_w^2) \quad \text{as} \quad \theta_w \to 0. \tag{2.3}$$

This limit allows for a competition between the effects of weak nonlinearity and diffraction, and is the one we consider in the present work. Morawetz (1994) has also analysed weak shock reflection in the transitional limit (2.3).

In figure 1, we illustrate the structure of the leading-order approximation of the flow. The method of matched asymptotic expansions shows that there are three main regions to consider.

I. Over most of the flow field, linearized theory is valid. The leading-order approximation satisfies a wave equation.

II. Near the reflection point, the leading-order approximation satisfies a two-dimensional inviscid Burgers equation.

III. At the edge of the diffracted wave, there is a very weak shock. The leading-order approximation near the diffracted shock satisfies a one-dimensional, cylindrical inviscid Burgers equation.

In the reflection region II, the leading-order asymptotic solution depends on a single dimensionless parameter a, which we define by

$$a = \frac{\theta_w}{2\sqrt{M-1}}, \tag{2.4}$$

where θ_w is measured in radians. For example, the numerical solution of the Euler equations shown in figure 7 of Colella & Henderson (1990), with $M = 1.0483$ and $\theta_w = 10°$, corresponds to $a = 0.40$. The experiment shown in figure 1 of Sasoh, Takayama & Saito (1992), with $M = 1.15$ and $\theta_w = 15°$, corresponds to $a = 0.34$, and the experimental observation of White, reproduced in figure 17 of Ben-Dor & Glass (1979), with $M = 1.01$ and $\theta_w = 5.7°$, corresponds to $a = 0.50$.

The normalized asymptotic problem in region II consists of the two-dimensional Burgers equation in the half-plane $y > 0$,

$$\left.\begin{array}{l} u_t + (\frac{1}{2}u^2)_x + v_y = 0, \\ u_y - v_x = 0. \end{array}\right\} \tag{2.5}$$

The independent variables x and y in (2.5) are scaled space variables parallel and normal to the surface of the wedge, respectively, in a reference frame moving with the sound speed ahead of the incident shock. The dependent variables u and v are scaled x and y velocity components, and pressure and density variations are proportional to u. If we consider an ideal fluid with density ρ, velocity $\boldsymbol{u}$, pressure p, and constant ratio γ of specific heats, then

$$\begin{pmatrix} \rho \\ \boldsymbol{u} \\ p \end{pmatrix} = \begin{pmatrix} \rho_0 \\ \boldsymbol{0} \\ p_0 \end{pmatrix} + \varepsilon \frac{2}{\gamma+1} u \begin{pmatrix} \rho_0 \\ c_0 \boldsymbol{e}_{\widetilde{x}} \\ \gamma p_0 \end{pmatrix} + \varepsilon^{3/2} \frac{2\sqrt{2}}{\gamma+1} v \begin{pmatrix} 0 \\ c_0 \boldsymbol{e}_{\widetilde{y}} \\ 0 \end{pmatrix} + O(\varepsilon^2), \tag{2.6}$$

where the small parameter ε is defined by

$$\varepsilon = 2(M-1), \tag{2.7}$$

and p_0, ρ_0, and c_0 are the pressure, density, and sound speed of the undisturbed fluid ahead of the incident shock. The variables $\widetilde{x}$ and $\widetilde{y}$ are spatial variables tangent and normal to the surface of the wedge, respectively, with corresponding unit coordinate vectors $\boldsymbol{e}_{\widetilde{x}}$ and $\boldsymbol{e}_{\widetilde{y}}$. The asymptotic space–time variables (x, y, t) are defined by

$$x = \frac{\widetilde{x} - c_0\widetilde{t}}{\varepsilon}, \quad y = \sqrt{2}\frac{\widetilde{y}}{\varepsilon^{1/2}}, \quad t = c_0\widetilde{t}, \tag{2.8}$$

where $\widetilde{t}$ is the physical time variable.

The initial condition for (2.5) is

$$u(x, y, 0) = \begin{cases} 0, & x > ay \\ 1, & x < ay. \end{cases} \tag{2.9}$$

Thus, the incident shock has strength one and is initially located at $x = ay$. The no-flow boundary condition on the wedge wall $y = 0$ implies that

$$v(x, 0, t) = 0. \tag{2.10}$$

Finally, the state ahead of the incident shock is undisturbed, so that

$$v(x, y, t) = 0 \quad \text{for} \quad x > s(y, t), \tag{2.11}$$

where $x = s(y, t)$ is the location of the incident and the Mach shocks.

The boundary condition in (2.10) can be replaced by the symmetry condition

$$u(x, -y, t) = u(x, y, t), \qquad v(x, -y, t) = -v(x, y, t).$$

The shock reflection problem is therefore equivalent to a one-parameter family of three-state Riemann problems. See Čanić & Keyfitz (1998) and Čanić & Mirković (1998) for a study of more general Riemann problems for (2.5). Numerical solutions of a related problem, the adjustment to steady state of a suddenly deflected transonic flow past a wedge, are given in Cole, Cook & Schleiniger (1997).

An algebraic analysis of the jump conditions for the two-dimensional Burgers equation shows that the regular reflection of plane shocks is impossible for $a < a_d$, where the detachment point a_d is given by (Hunter 1991)

$$a_d = \sqrt{2}. \tag{2.12}$$

The two-dimensional Burgers equation does not have triple-point solutions in which three plane shocks separated by constant states meet at a point (Brio & Hunter 1992; Tabak & Rosales 1994). Thus, a standard single Mach reflection cannot occur when regular reflection becomes impossible, and the asymptotic problem embodies the 'triple-point paradox' of weak shock reflection in its most basic form.

A second significant value of a for transition is the sonic point a_s, where

$$a_s = \sqrt{1 + \sqrt{5}/2}, \tag{2.13}$$

at which the reflection point is exactly sonic with respect to the flow behind the reflected shock (Brio & Hunter 1992). The sonic point $a_s \approx 1.455$ is slightly larger than the detachment point $a_d \approx 1.414$.

3. Numerical results

Numerical solutions of the asymptotic shock reflection problem (2.5), (2.9)–(2.11) show a transition from regular to Mach reflection as a decreases below a critical value that is close to the sonic and detachment points (2.12)–(2.13). We found that the structure of the Mach reflection near the triple point is easier to resolve for a close to 0.5 than for other values of a. When a is larger than 0.5, the size of the structure that must be resolved near the triple point seems to be even smaller than for $a = 0.5$ (see figure 8, for example). Moreover, the triple point moves up the Mach shock more slowly with increasing values of a, so that longer computing times are required to obtain the same numerical resolution. When a is smaller than 0.5, the reflected shock becomes extremely weak and its numerical shock thickness becomes large, so that the structure of the solution near the triple point is smeared out.

In figures 2 and 3 we show a numerical solution of (2.5), (2.9)–(2.11) which gives an overall picture of the irregular reflection for $a = 0.5$. The u-contours, which correspond to density and pressure contours, are in qualitative agreement with those of experimentally observed shock reflections (see figure 18 in Bleakney & Taub 1949, for example). The solution closely resembles a single Mach reflection. The triple-point location is $y/t \approx 0.51$. The strength of the incident shock, measured by the jump in u, is equal to 1. The strength of the Mach shock increases as it moves away from
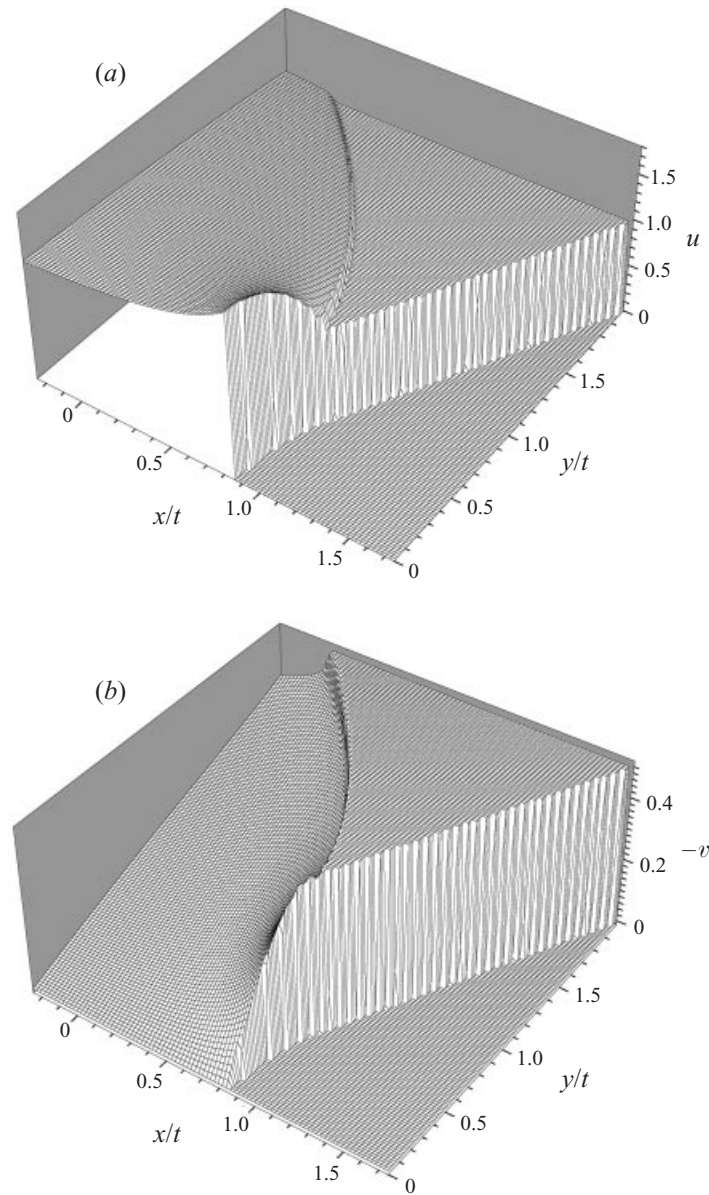
FIGURE 2. A surface plot of (a) u and (b) $-v$ for $a = 0.5$.

the triple point and reaches 1.8 at the wall. The reflected shock is much weaker than the incident shock, with a strength of approximately 0.07 at the sonic point on the reflected shock. Plots of the incident Mach shock strength and the reflected shock strength as functions of y/t are shown in figure 4. The strength of the reflected shock at the triple point is difficult to estimate from figure 4(b) because, very close to the triple point, the numerically computed jump may include a contribution from part of an expansion fan as well as the jump across the reflected shock.

Figure 5 shows a numerical solution of u and v near the triple point. The dotted line is the numerically computed location of the sonic line (4.2) where the self-similar
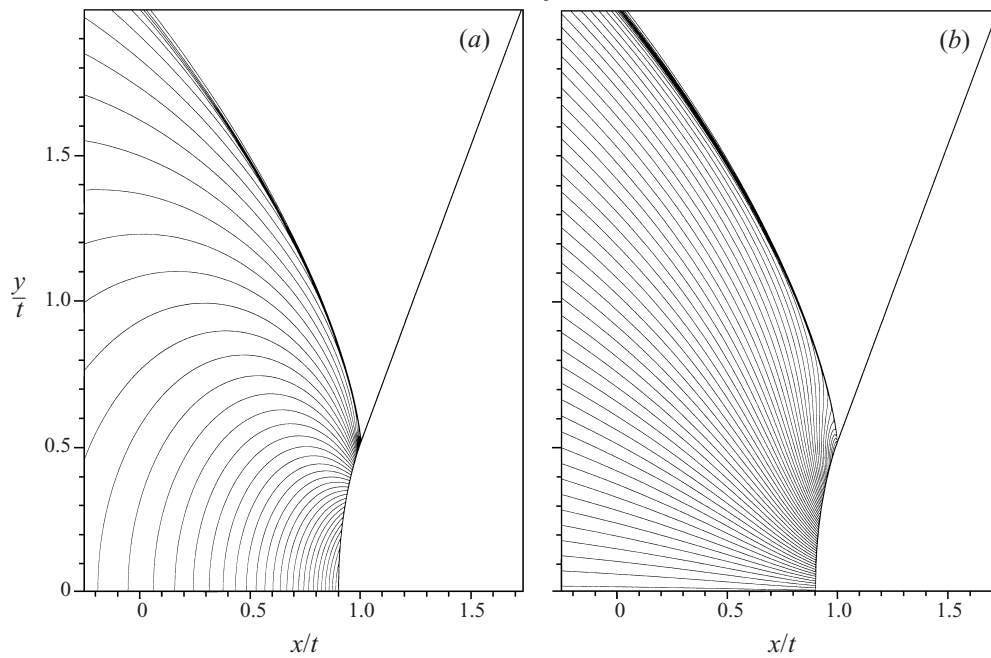
FIGURE 3. A contour plot of (*a*) *u* and (*b*) *v* for *a* = 0.5. The *u*-contour spacing is 0.02 and the *v*-contour spacing is 0.01. The region shown in figures 2 and 3 is covered by a 3600 × 1800 grid which is cut out from a larger 6000 × 2400 grid to remove numerical boundary effects. The *y*-grid spacing is twice the *x*-grid spacing and the time step is one half of the *x*-grid spacing. The total number of time steps is 3600.
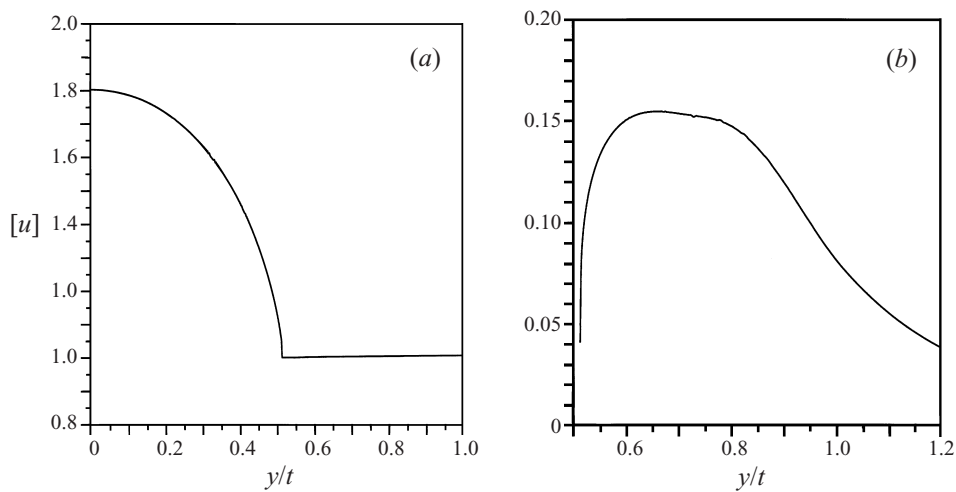

FIGURE 4. The strength of (*a*) the incident shock and the Mach shock, and (*b*) the reflected shock, measured by the jump in *u*, as a function of *y*/*t*. The jump is computed across a numerical shock profile of six grid points in *x*/*t* in (*a*) and eight in (*b*).

equations change type. The sonic line bends back into the reflected wave and there is a very small supersonic patch behind the triple point. The supersonic patch is approximately 0.0015 wide in *x*/*t* and 0.006 high in *y*/*t*. This height is approximately 1% of the height of the Mach shock.
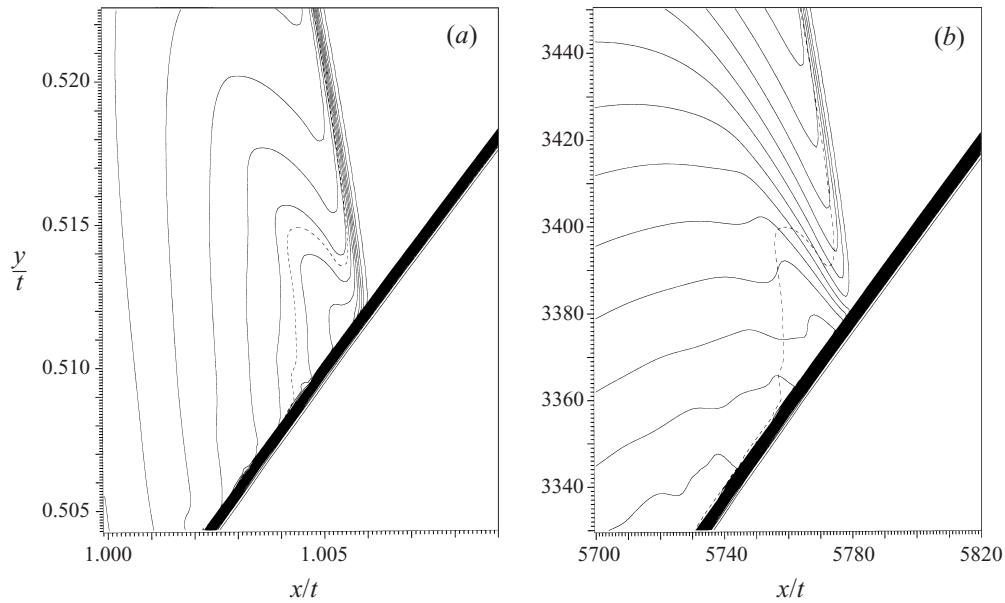
FIGURE 5. A contour plot of (*a*) *u* and (*b*) *v* near the triple point for $a = 0.5$. The *u*-contour spacing is 0.01 in (*a*) and the *v*-contour spacing is 0.002 in (*b*). The dotted line is the sonic line. The region shown here is 120×120 grid points wide, and is cut out from a solution computed on a 7200×4800 grid after 26400 time steps. In (*b*) the axes are labelled by grid point number.
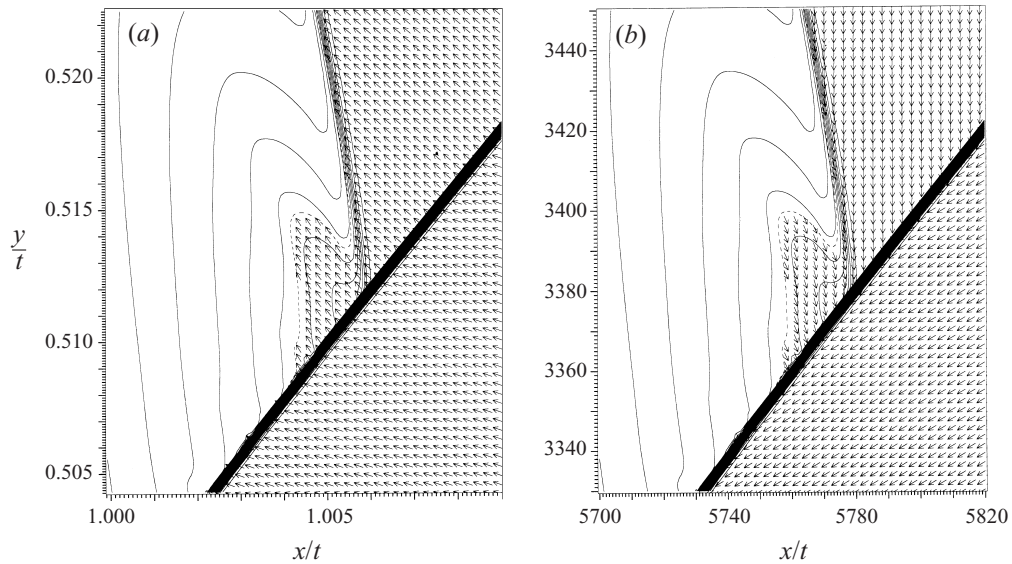

FIGURE 6. (*a*) The minus and (*b*) the plus characteristic vector field near the triple point for $a = 0.5$.

The self-similar equations have two families of characteristics in the supersonic region, whose slopes are given in (4.3). Figure 6 shows the numerically computed characteristic vector fields of the solution inside the supersonic patch. The implications of figure 6 for the structure of the solution are discussed in §4.

The region shown in figures 5 and 6 is 120×120 grid cells wide, and is cut out from

a solution computed on a 7200×4800 grid. The supersonic patch is approximately 20×40 grid points wide and is well separated from the incident and reflected shocks, which are about 5 grid points wide. A rough measure of the resolution of a numerical solution of a Mach reflection on a uniform grid is provided by the number (N_x, N_y) of (x, y)-grid points between the reflection point where the Mach shock hits the wedge and the triple point. In this computation, we have $(N_x, N_y) \approx (1350, 3380)$. The grids used in previous numerical solutions of weak shock reflection were not fine enough to resolve the supersonic patch. For example, the solution of the full Euler equations shown in figure 7 of Colella & Henderson (1990) has $(N_x, N_y) \approx (20, 300)$, while the solution of the two-dimensional Burgers equation shown in figure 22 of Tabak & Rosales (1994), has $(N_x, N_y) \approx (15, 100)$.

If the size of the supersonic patch is $\Delta\xi$ in x/t and $\Delta\eta$ in y/t, then (2.7) and (2.8) imply that the size of the patch in physical variables is

$$\Delta\widetilde{x} \sim 2(M-1)c_0\widetilde{t}\Delta\xi, \qquad \Delta\widetilde{y} \sim (M-1)^{1/2}c_0\widetilde{t}\Delta\eta. \qquad (3.1)$$

As $M \to 1$, the distance travelled by the reflection point along the wedge wall approaches $c_0\widetilde{t}$. For a Mach number of 1.04 and a wedge angle of $11.5°$, we have $a = 0.5$, $\Delta\xi \approx 0.0015$, and $\Delta\eta \approx 0.006$. Equation (3.1) then gives the estimate of the patch size stated in the introduction.

If the triple point in the solution of the two-dimensional Burgers equation is located at $y/t = \eta_*$, then the angle χ between the triple-point trajectory and the wedge wall is given by

$$\chi \sim \frac{\eta_*\theta_w}{2a} \quad \text{as} \quad \theta_w \to 0 \quad \text{with } a \text{ fixed.}$$

From the numerical solution, it follows that $\chi \sim (0.51)\theta_w$ when $a = 0.5$.

In figure 7 we show a numerical solution of (2.5) with the initial data

$$u(x, y, 0) = \begin{cases} 0, & x > \alpha y \\ u_0, & x < \alpha y, \end{cases} \qquad (3.2)$$

where $\alpha = 0.5$ and $u_0 = 0.390625$. The change of variables

$$u \to \frac{u}{u_0}, \quad v \to \frac{v}{u_0^{3/2}}, \quad x \to \frac{x}{u_0}, \quad y \to \frac{y}{u_0^{1/2}}, \quad t \to t,$$

leaves (2.5) invariant and transforms (3.2) to (2.9) with

$$a = \alpha u_0^{-1/2}.$$

Thus, after a rescaling, this problem is equivalent to the case $a = 0.8$.

The triple point is located at $y/t \approx 0.14$, which gives $\chi \sim (0.14)\theta_w$. The strength of the Mach shock at the wall is 2.5 times the incident shock strength. A distinctive feature of the solution is a sharp minimum in the y-velocity component v just behind the triple point. This feature was observed in Tabak & Rosales (1994) (see figure 38, which corresponds to $a = 0.79$). The minimum is caused by the opposing effects of changes in the strength and slope of the Mach shock. Initially, v becomes more negative because the Mach shock gets rapidly stronger as it moves away from the triple point. After the minimum, v increases back towards zero as the Mach shock becomes more vertical. Another interesting feature of the solution is that the reflected shock becomes vertical just before it hits the incident shock, then bends around so that it is sloping forwards in the reference frame of the wedge at the triple point.
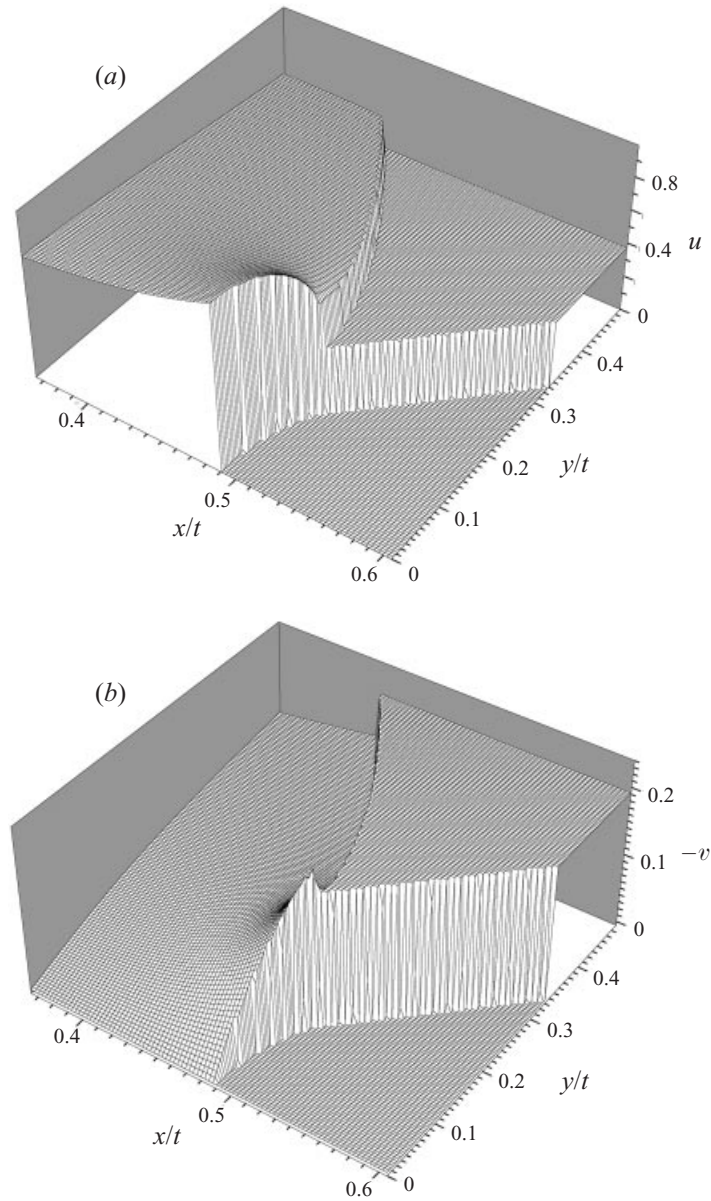
(a)

(b)

FIGURE 7. A surface plot of (a) u and (b) $-v$ for (2.5) with initial data (3.2) where $\alpha = 0.5$, $u_0 = 0.390625$, and $a = 0.8$. The region shown in the figure is covered by a uniform 1800×1800 grid.

Figure 8 shows the v-contours near the triple point. The numerical solution is not sufficiently resolved to show the structure of the solution at the triple point.

4. Theoretical discussion

In this section, we use various theoretical considerations to interpret the numerical solutions shown in §3. The result is the structure illustrated schematically in figure 9.
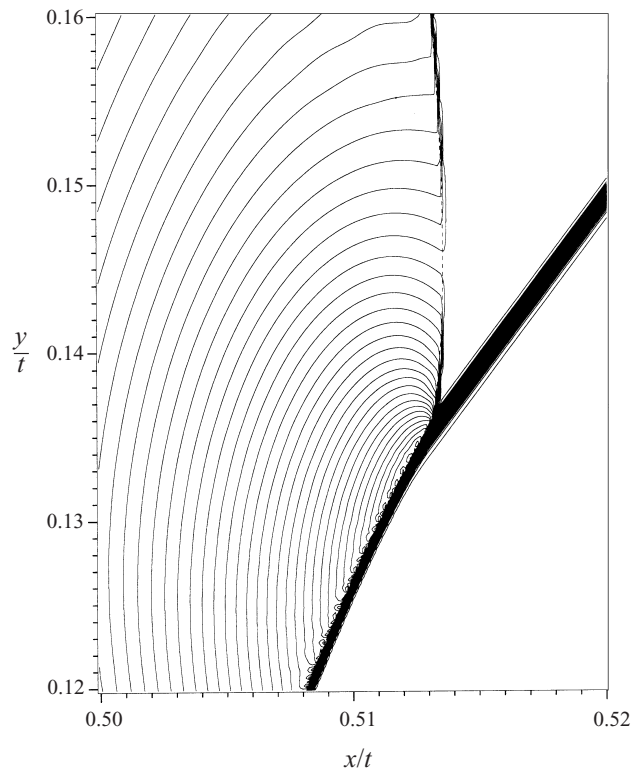
FIGURE 8. A contour plot of v near the triple point for (2.5) with initial data (3.2) where $\alpha = 0.5$, $u_0 = 0.390625$, and $a = 0.8$. The v-contour spacing is 0.002 and the dotted line is the sonic line. The region shown is 173×173 grid points wide.

In self-similar variables,

$$\xi = \frac{x}{t}, \qquad \eta = \frac{y}{t},$$

the two-dimensional Burgers equation (2.5) becomes

$$\left.\begin{array}{l} -\xi u_\xi - \eta u_\eta + (\tfrac{1}{2}u^2)_\xi + v_\eta = 0, \\ u_\eta - v_\xi = 0. \end{array}\right\} \tag{4.1}$$

This equation is hyperbolic when $u < \xi + \eta^2/4$ and elliptic when $u > \xi + \eta^2/4$. The location of the sonic line where (4.1) changes type is given by

$$u(\xi, \eta) = \xi + \tfrac{1}{4}\eta^2. \tag{4.2}$$

In the supersonic, hyperbolic region, the inverse slopes of the characteristic curves of (4.1) are given by

$$\left(\frac{\mathrm{d}\xi}{\mathrm{d}\eta}\right)_c = -\tfrac{1}{2}\eta \pm \sqrt{\xi + \tfrac{1}{4}\eta^2 - u}. \tag{4.3}$$

We call the characteristics plus or minus characteristics depending on the choice of sign in this equation. The direction of propagation along the self-similar characteristics can be determined by a consideration of the domain of dependence of the time-dependent equations, and is in the direction of decreasing $\xi + \eta^2/4$. Equivalently, η increases along the minus characteristics and decreases along the plus characteristics.
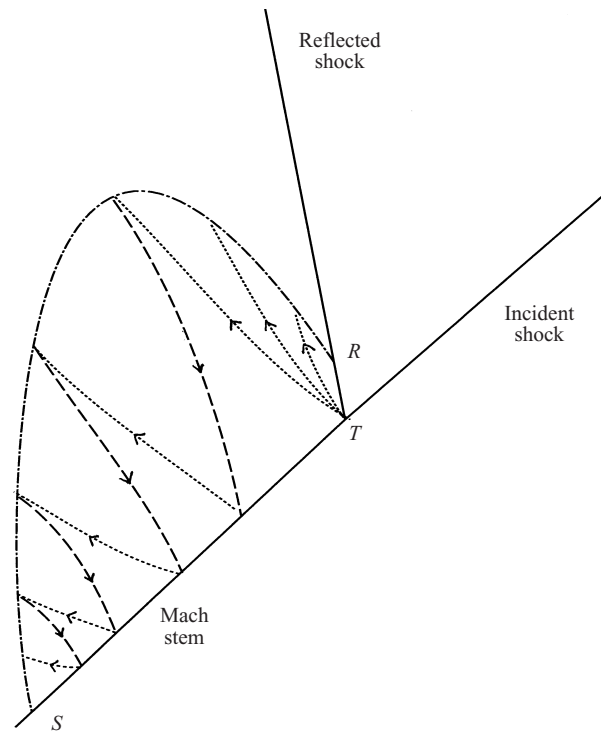
FIGURE 9. A schematic diagram of the structure of weak-shock irregular reflection. The dotted-dashed line is the sonic line, the dotted lines are minus characteristics, the dashed lines are plus characteristics, R is the sonic point on the reflected shock, S is the sonic point on the Mach stem, and T is the triple point. The limiting case in which $R = T$ is not excluded.

In the numerical solution for $a = 0.5$ shown in figure 5, the reflected shock appears to overtake the incident shock at a triple point, and there is a supersonic patch behind the triple point. From figure 6, the plus characteristics converge on the reflected shock, the incident shock, and the Mach shock from either side, while the minus characteristics cross the shocks, so all the shocks are plus shocks.

A conceivable alternative to the existence of a triple point is that the reflected shock strength tends to zero at some point P before it hits the incident shock, so that the reflected wave is continuous after P. The following considerations, however, make it difficult to construct a plausible structure in which this could happen.

First, if the reflected shock enters the supersonic region, then, from the direction of propagation of the characteristics shown in figure 6(*b*), the point P is not a shock formation point, but a point at which the reflected shock disappears. Shocks in solutions of hyperbolic conservation laws typically remain in existence once they have formed, so this behaviour is inconsistent with the expected qualitative properties of the self-similar equations. Although we do not know of a rigorous proof of the persistence of shocks that is applicable to the two-by-two system of self-similar equations in the hyperbolic region, we solved numerically a number of initial value problems for these equations with hyperbolic initial data that consisted of two shocks in the same family. Depending on the strength and location of the initial shocks, we observed the overtaking of one shock by another, with the generation of a reflected expansion fan, or the collision of a shock with the sonic line before overtaking occurred. We never observed the disappearance of a shock in the hyperbolic region.

Second, if part of the reflected wave near the apparent triple point is continuous and bounded by the sonic line, then the sonic line propagates into the state $u = 1$ behind the incident shock. Consequently, the parabola given by the sonic line equation (4.2) with $u = 1$ is close to the apparent triple point on the incident shock. This parabola, however, intersects the incident shock, located at $\xi = a\eta + a^2 + 1/2$, at $\eta = \sqrt{2} - 2a$. For $a = 0.5$, this gives $\eta \approx 0.41$, which is well below the numerically computed location $\eta \approx 0.51$ of the apparent triple point. The discrepency between the location of the triple point and the location of a sonic line propagating into the state behind the incident shock was noted previously in Tabak & Rosales (1994).

From figure 5(a), the numerically computed location of the sonic point behind the reflected shock is given by $(\xi, \eta) \approx (1.0055, 0.514)$. This location is close to the triple point, and is consistent with (4.2), because $u \approx 1.07$ at the sonic point behind the reflected shock. This state is more compressed than the state behind the incident shock, so the sonic line propagates faster than it would into the state behind the incident shock.

These considerations support the numerical observation that the reflected shock hits the incident shock at a triple point. Given that the incident and reflected shocks are separated by smooth states, belong to the same family, and merge at a supersonic point, we can determine theoretically the waves produced after they merge by solving a local Riemann problem for the two-by-two system of self-similar equations. As we will show, the waves produced are a Mach shock in the same family as the incident and reflected shocks, and a reflected expansion fan in the opposite family.

To carry out this analysis, we transform (2.5) into a reference frame in which the triple point is at rest and examine the shock and rarefaction curves of the steady equations. The incident shock is given by

$$\left. \begin{array}{lll} u = 0, & v = 0, & x > s(y, t), \\ u = 1, & v = -a, & x < s(y, t), \\ s(y, t) = ay + (a^2 + \tfrac{1}{2})t. & & \end{array} \right\} \tag{4.4}$$

We denote the position of the triple point by

$$x = \xi_* t, \qquad y = \eta_* t,$$

where the constants ξ_* and η_* satisfy

$$\xi_* = a\eta_* + a^2 + \tfrac{1}{2}.$$

The following transformation leaves the two-dimensional Burgers equation invariant and reduces the triple point to rest:

$$\bar{x} = x + \tfrac{1}{2}\eta_* y - (\xi_* + \tfrac{1}{2}\eta_*^2)t, \quad \bar{y} = y - \eta_* t,$$

$$\bar{u} = u - (\xi_* + \tfrac{1}{4}\eta_*^2), \quad \bar{v} = v - \tfrac{1}{2}\eta_* u.$$

The triple point is located at the origin of the barred coordinates, and the incident shock position is

$$\bar{x} = \bar{a}\bar{y},$$

where

$$\bar{a} = a + \tfrac{1}{2}\eta_*.$$

In the barred reference frame, the states (u_1, v_1) ahead of the incident shock and (u_2, v_2) behind the incident shock are given by

$$u_1 = -(\tfrac{1}{2} + \bar{a}^2), \qquad v_1 = 0,$$

$$u_2 = \tfrac{1}{2} - \bar{a}^2, \qquad v_2 = -\bar{a}.$$

Dropping the bars, and assuming that the flow near the triple point is approximately steady, we may consider solutions of the steady two-dimensional Burgers equation, or steady transonic small disturbance equation,

$$\left. \begin{array}{l} (\tfrac{1}{2}u^2)_x + v_y = 0, \\ u_y - v_x = 0. \end{array} \right\} \tag{4.5}$$

The shock curve of (4.5) of left-hand states (u, v) which are connected by a shock to a right-hand state (u_R, v_R) is (Cole & Cook 1986)

$$\tfrac{1}{2}(u - u_R)^2(u + u_R) + (v - v_R)^2 = 0,$$

with $u > u_R$. The shock is forward facing if $v < v_R$ and backward facing if $v > v_R$. The rarefaction curves through the right-hand state (u_R, v_R) are given by

$$v = v_+ + \tfrac{2}{3}(-u)^{3/2}, \qquad v = v_- - \tfrac{2}{3}(-u)^{3/2},$$

with $u < u_R < 0$, where

$$v_+ = v_R - \tfrac{2}{3}(-u_R)^{3/2}, \qquad v_- = v_R + \tfrac{2}{3}(-u_R)^{3/2}.$$

The expansion wave is forward facing if $v > v_R$, corresponding to v_+, and backward facing if $v < v_R$, corresponding to v_-.

The shock and rarefaction curves for a triple point with three forward facing shocks and one backward facing expansion wave are shown in figure 10 for $a = 0.5$. In this plot, the jump in u across the incident shock is 1, the jump in u across the reflected shock is 0.05, and $\eta_* = 0.5$. The change in u across the expansion fan is then 0.02, and the jump in u across the Mach stem is 1.03. The dip of the u-contours towards the sonic point in figure 5(a) is consistent with the presence of a minus expansion fan originating at the triple point, whose corner is smoothed out by numerical diffusion.

The leading-order asymptotic solution is isentropic and irrotational, but shocks generate higher-order entropy and vorticity perturbations. From the weak shock expansion of the jump conditions for the Euler equations, Whitham (1974, p. 176), and equation (2.6), the entropy jump $[S]$ across a shock is third order in the shock strength, and is given in terms of the jump $[u]$ in the asymptotic variable u by

$$\frac{[S]}{c_v} = \frac{2\gamma(\gamma - 1)}{3(\gamma + 1)^2} \varepsilon^3 [u]^3 + O(\varepsilon^4),$$

where c_v is the specific heat at constant volume. For the shock strengths observed in the numerical solution, it follows that the entropy jump at the triple point across the Mach shock is greater than the sum of the entropy jumps across the incident and the reflected shocks. Since there is no change in entropy across an expansion fan, the corresponding triple-point solution of the Euler equations must contain a very weak contact discontinuity of strength $O(\varepsilon^3)$, in addition to the weak expansion fan and the three weak shocks of strength $O(\varepsilon)$. For an analysis of the entropy jumps across shocks at a triple point in fluids with a convex equation of state, see Henderson & Menikoff (1998).

The origin of the non-uniform wave inside the supersonic patch may be explained by the reflection of characteristics off the sonic line. From (4.3) both families of characteristics have the same inverse slope on the sonic line,

$$\left(\frac{\mathrm{d}\xi}{\mathrm{d}\eta} \right)_c = -\tfrac{1}{2}\eta.$$

Differentiation of equation (4.2) for the sonic line with respect to ξ gives the sonic
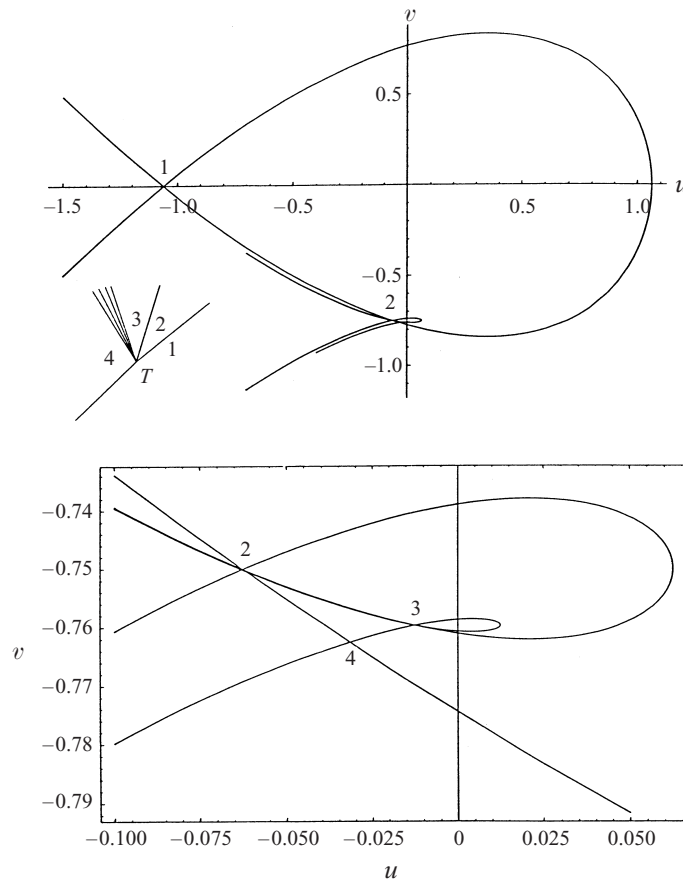
FIGURE 10. A plot of the shock and rarefaction curves for a triple point with an expansion fan. The state ahead of the incident shock is denoted by 1, the state between the incident and reflected shocks by 2, the state behind the reflected shock by 3, and the state behind the Mach stem by 4.

line slope,

$$\left(\frac{\mathrm{d}\xi}{\mathrm{d}\eta}\right)_s = \frac{-\frac{1}{2}\eta + u_\eta}{1 - u_\xi}.$$

The characteristics are tangent to the sonic line if and only if

$$\tfrac{1}{2}\eta u_\xi = u_\eta.$$

This condition is satisfied if u is constant ahead of the sonic line. In that case, both families of characteristics propagate towards the sonic line and no disturbance in the subsonic region can influence the solution in the supersonic region. The tangency of the characteristics to the sonic line is broken when the sonic line is embedded inside a non-uniform wave (Brio & Hunter 1995) thus allowing the reflection of characteristics off the sonic line, and the generation of a supersonic wave.

As illustrated in figure 9, the supersonic patch, the supersonic part of the reflected shock, and the supersonic part of the Mach shock are all influenced by plus characteristics that originate at the sonic line. The structure is therefore consistent with domain of dependence arguments which imply that a non-uniform wave or a curve in the incident or reflected shocks cannot form in any part of the hyperbolic region

where both families of characteristics can be traced back through the hyperbolic region to infinity (Tabak & Rosales 1994).

In the case of steady shock reflection, Guderley (1962, p. 149), showed that the sonic line must pass exactly through the triple point. His argument, for the steady transonic small-disturbance equations, is that the plus wave is reflected off the sonic line as a compression wave. If the reflected plus shock had a supersonic section, then its strength would increase as it absorbed the plus compression wave, in contradiction to the fact that its strength must decrease as the flow behind it changes from subsonic to supersonic. This argument is not applicable to the self-similar equations. We do not know of any reason why the sonic line must pass exactly through the triple point in the self-similar case, meaning that $R = T$ in figure 9, although this limiting case is not excluded by the numerical solutions or theoretical arguments.

The existence of a supersonic patch behind the triple point raises some subtle questions connected with the 'transonic controversy' concerning shock-free flow transonic flows over airfoils. At a given free-stream Mach number, special airfoil shapes allow steady transonic shock-free flow, but the flow typically does not remain shock-free if the shape of the airfoil is perturbed (Morawetz 1956*a–c*, 1982). The supersonic patch is analogous to the supersonic bubble on a transonic airfoil, although an argument like the one in Morawetz (1956*a–c*) would not establish the impossibility of shock-free flow in the patch because the Mach shock is a free boundary whose shape varies with the Mach number of the incident shock.

The supersonic bubble in a transonic flow over an airfoil is typically terminated by a shock. If there were a shock at the rear of the supersonic patch behind the triple point, then there would be two triple points: the leading supersonic triple point and a trailing triple point. Subsonic triple points that satisfy a few mild conditions are impossible for the unsteady transonic small-disturbance equation (Gamba, Rosales & Tabak 1999) so there would presumably be a second supersonic patch behind the trailing triple point, and therefore a second expansion fan. In that case, there would be a finite or infinite sequence of supersonic triple points, minus expansion fans and plus shocks reflected between the Mach shock and the sonic line, and a complicated singularity at the rear of the supersonic patch. The resolution of the numerical results presented here is not sufficient to determine whether or not the flow behind the Mach shock is shock-free.

5. The numerical scheme

The asymptotic shock reflection problem consists of equations (2.5), (2.9)–(2.11). To solve this problem numerically, we first obtain a set of equations for u. We eliminate v from the differential equations (2.5) by cross-differentiation, and from the boundary condition (2.10) by differentiation with respect to x and use of the irrotationality condition $v_x = u_y$, which gives $u_y = 0$ on $y = 0$. Equations (2.5), (2.9)–(2.11) imply that $u = 0$ ahead of the incident and the Mach shocks. It is convenient to make a Galilean transformation $x \to x + ct$, $y \to y$, where

$$c = \tfrac{1}{2} + a^2,$$

into a reference frame moving with the incident shock. This Galilean transformation has been removed in the numerical solutions shown in §3. The resulting initial-
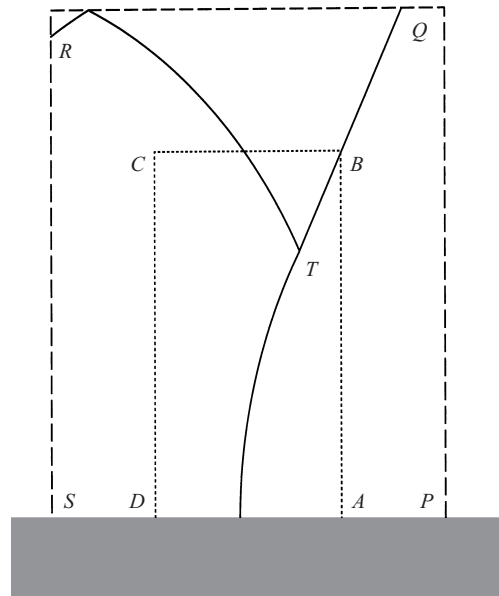
FIGURE 11. A schematic diagram of the grid in the (x, y)-plane used in the numerical solution. The dashed line $PQRS$ is the boundary of the computational domain. The dotted line $ABCD$ encloses the region where a uniform grid is used, with an exponentially stretched grid outside. The fine grid computation is stopped when the triple point T is close to the edge of the uniform grid.

boundary value problem in $y > 0$ for $u(x, y, t)$ may then be written as

$$
\left.
\begin{aligned}
&(u_t + f(u)_x)_x + u_{yy} = 0, \\
&u(x, y, 0) = \begin{cases} 0, & x > ay \\ 1, & x < ay, \end{cases} \\
&u_y(x, 0, t) = 0, \\
&u(x, y, t) = 0 \quad \text{for} \quad x > s(y, t),
\end{aligned}
\right\}
\tag{5.1}
$$

where $x = s(y, t)$ is the location of the incident and the Mach shocks, and the flux function $f(u)$ is given by

$$
f(u) = \tfrac{1}{2}(u - c)^2.
\tag{5.2}
$$

We recover v from u by integration with respect to x,

$$
v(x, y, t) = -\int_x^\infty u_y(x', y, t)\, dx'.
$$

In transonic computations, the introduction of a velocity potential is more usual than the elimination of v, but in this problem both methods lead to equivalent results.

When solving the half-space problem (5.1) numerically, we use the finite computational domain shown schematically in figure 11. We choose the domain so that the incident shock leaves through the top boundary, and we stop the computation soon after the reflected shock hits the top boundary. In addition to the physical boundary condition $u_y = 0$ on the wall $y = 0$, we require numerical boundary conditions on the computational boundaries. We impose $u = 0$ on the right-hand boundary PQ, and
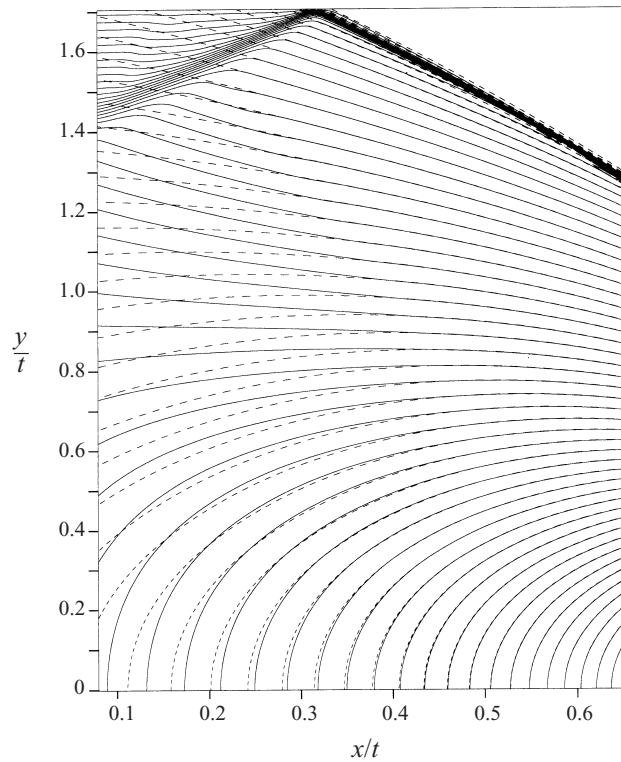
FIGURE 12. A comparison of the *u*-contours near the left and top computational boundaries of the fine grid solution (solid lines) with the *u*-contours from the solution shown in figure 3 computed on a much larger computational domain (dashed lines).

the Dirichlet condition

$$u(x, y, t) = \begin{cases} 0, & x > ay \\ 1, & x < ay, \end{cases} \qquad (5.3)$$

corresponding to the unperturbed incident shock, on the top boundary QR. The boundary which causes the greatest numerical difficulties is the left-hand boundary RS. This is an inflow boundary, and the solution is unknown on the subsonic part of it. We therefore use a non-reflecting boundary condition (Enquist & Majda 1981) on the left-hand boundary, and we found that linear extrapolation, $u_x = 0$, was reasonably effective. Nevertheless, a numerical wave is generated at the lower-left corner S and propagates into the computational domain. To avoid pollution of the solution by boundary waves, we use an exponentially stretched grid near the left-hand, right-hand, and top boundaries (see figure 11). In the fine grid computation, we use a stretching factor of 0.25% per grid cell. We stop the computation before any boundary waves propagate into the reflection region, and before the triple point leaves the region covered by the uniform, unstretched grid.

In figure 12, we compare the *u*-contours in the left-hand part of the computational domain of the fine grid solution, from which the triple-point solutions in figures 5 and 6 are extracted, with the *u*-contours of the solution shown in figures 2 and 3, which is computed on a much larger domain to ensure the elimination of boundary effects. The distortion of the *u*-contours of the fine grid solution by the corner wave

can be seen in figure 12, but the fine grid contours coincide with the large domain contours for $x/t \geqslant 0.6$, which includes the reflection region.

The most important feature of the finite difference scheme that we use to solve (5.1) is the time discretization. Denoting an approximation of the solution at the time level n by

$$u^n(x, y) \approx u(x, y, n\Delta t),$$

where Δt is the time step, we discretize (5.1) in time as follows:

$$\left[\frac{u^{n+1} - u^n}{\Delta t} + f(u^n)_x\right]_x + u_{yy}^{n+1} = 0. \tag{5.4}$$

This scheme is similar to one introduced by Ballhaus & Lomax (1975) (see also Steger & Dalsen 1989) for unsteady transonic flow computations. The implicit time discretization of the diffraction term u_{yy} leads to a stable numerical scheme.

Equation (5.4) is a heat equation for $u^{n+1}(x, y)$, with diffusivity Δt, in which $-x$ is a time-like variable and y is a space-like variable. The condition $u = 0$ on the right-hand boundary PQ in figure 17 gives 'initial' data in $-x$ for (5.4). The boundary conditions in y are the Neumann condition $u_y = 0$ on $y = 0$ and the Dirichlet condition (5.3) on the top boundary.

We solve (5.4) by means of a fully implicit scheme to minimize numerical oscillations, sweeping from right to left in x. Specifically, if

$$u_{i,j}^n \approx u^n(i\Delta x, j\Delta y),$$

where Δx and Δy are the x and y grid spacing, respectively, we use a spatial discretization of (5.4) of the form

$$u_{i,j}^{n+1} - \sigma(u_{i,j+1}^{n+1} - 2u_{i,j}^{n+1} + u_{i,j-1}^{n+1})$$
$$= u_{i+1,j}^{n+1} + u_{i,j}^n - u_{i+1,j}^n + v(f_{i+3/2,j}^n - f_{i+1/2,j}^n - f_{i-1/2,j}^n + f_{i-3/2,j}^n), \tag{5.5}$$

where

$$v = \frac{\Delta t}{\Delta x}, \qquad \sigma = \frac{\Delta t \Delta x}{\Delta y^2}.$$

For the numerical flux function $f_{i-1/2,j}^n$ in (5.5), we use a min-mod flux-limiter (Yang & Przekwas 1992) that interpolates between the Enquist–Osher and Lax–Wendroff fluxes associated with the flux $f(u)$ in (5.2). Dropping the t-superscript n and the y-subscript j, which are fixed throughout the following expressions, this numerical flux is given by

$$f_{i-1/2} = (1 - s_{i-1/2})f_{i-1/2}^{EO} + s_{i-1/2}f_{i-1/2}^{LW},$$

$$f_{i-1/2}^{EO} = \tfrac{1}{2}\max[u_{i-1} - c, 0]^2 + \tfrac{1}{2}\min[u_i - c, 0]^2,$$

$$f_{i-1/2}^{LW} = \tfrac{1}{4}[(u_{i-1} - c)^2 + (u_i - c)^2] + \tfrac{1}{2}v(u_{i-1} - u_i)v_{i-1/2}^2,$$

$$v_{i-1/2} = \tfrac{1}{2}(u_{i-1} + u_i) - c.$$

The flux-limiter $s_{i-1/2}$ is defined by

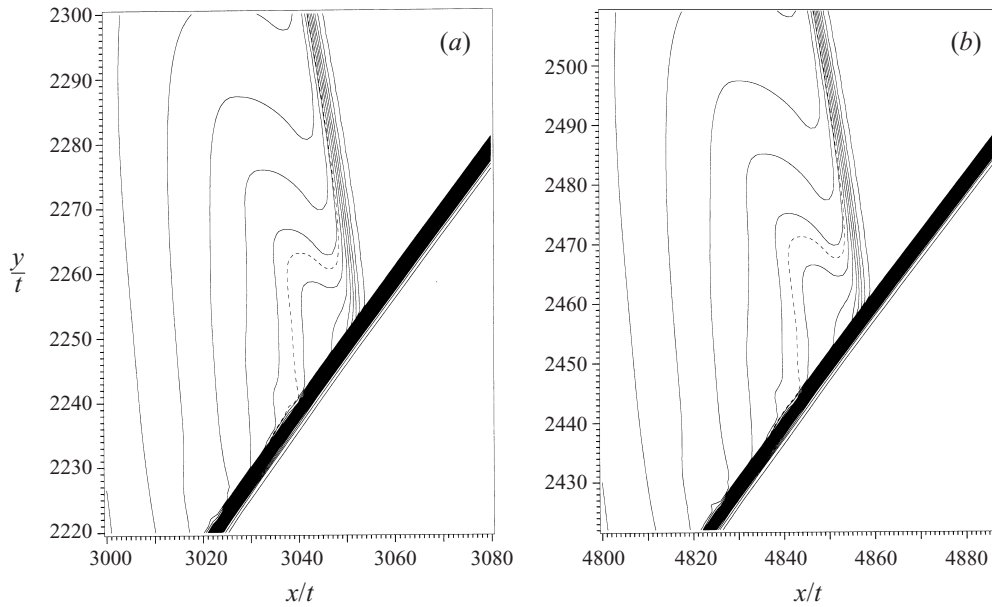$$s_{i-1/2} = \begin{cases} 0, & r_{i-1/2} \leqslant 0 \\ r_{i-1/2}, & 0 < r_{i-1/2} < 1 \\ 1, & r_{i-1/2} \geqslant 1, \end{cases}$$

FIGURE 13. A contour plot of u near the triple point for $a = 0.5$, from a solution on (*a*) a 4800×3200 grid after 17600 time steps, and (*b*) 7200×4800 grid after 19200 time steps. The dotted line is the sonic line, and the u-contour spacing is 0.01. The region of $(x/t, y/t)$-space shown here is the same as in figure 5(*a*).

$$r_{i-1/2} = \frac{[|v_{i-3/2}| - vv_{i-3/2}^2][u_{i-1} - u_{i-2}]}{[|v_{i-1/2}| - vv_{i-1/2}^2][u_i - u_{i-1}]} \quad \text{if} \quad v_{i-1/2} \geqslant 0,$$

$$r_{i-1/2} = \frac{[|v_{i+1/2}| - vv_{i+1/2}^2][u_{i+1} - u_i]}{[|v_{i-1/2}| - vv_{i-1/2}^2][u_i - u_{i-1}]} \quad \text{if} \quad v_{i-1/2} < 0.$$

This scheme is first-order accurate. We tried a number of schemes that were second-order accurate in time, using the time discretization

$$u_{yy} \approx \tfrac{1}{2}(u_{yy}^n + u_{yy}^{n+1}),$$

but found that they led to the generation of unacceptably large numerical oscillations at the shocks.

We carried out convergence studies to check that the numerical solutions are self-similar and that the supersonic patch is resolved. In figure 13(*a*), we show the u-contours in the same region of $(x/t, y/t)$ space that is shown in figure 5(*a*) from a computation on a coarser grid. In figure 13(*b*), we show the u-contours from the fine grid solution at an earlier time. The u-contours are in excellent quantitative agreement. The main effect of increasing numerical resolution is that the dip of the u-contours and the sonic line towards the triple point becomes more pronounced. The width of the shocks in x/t shrinks with increasing resolution, but the width of the supersonic patch remains the same.

6. Euler equations

In this section, we summarize the full shock reflection problem, and in subsequent sections we describe the systematic derivation of the asymptotic shock reflection

problem. The main point is the derivation of initial data for the two-dimensional Burgers equation by matching the weakly nonlinear solution with the linearized solution.

We neglect viscosity, and will not consider its effects on the ideal fluid description of shock reflection studied here. For simplicity, we suppose that the shock hits the wedge at a symmetric angle of incidence. An identical asymptotic problem in the reflection region is obtained for asymmetric incidence.

We denote spatial coordinates normal and tangent to the incident shock front by $\overline{x}$ and $\overline{y}$ and time by $\overline{t}$. We will use the following notation to distinguish between the different physical variables and asymptotic variables: for a variable z, such as a space coordinate or a velocity component,

$$\overline{z} = \text{original physical variable,}$$

$$\widetilde{z} = \text{physical variable in a rotated}$$

$$\text{coordinate system aligned with the wedge,}$$

$$\widehat{z} = \text{unnormalized asymptotic variable,}$$

$$z = \text{normalized asymptotic variable.}$$

The region Ω of the upper half-plane outside the wedge is given by

$$\Omega = \left\{ (\overline{x}, \overline{y}) : \theta_w < \overline{\theta} < \pi \right\},$$

where θ_w is the half-angle of the wedge, and $\overline{\theta}$ is the polar angle

$$\overline{\theta} = \tan^{-1}\left(\frac{\overline{y}}{\overline{x}} \right).$$

The fluid density ρ, velocity $\boldsymbol{u}$, and pressure p satisfy the two-dimensional compressible Euler equations,

$$\left. \begin{array}{l} \rho_{\overline{t}} + \nabla \cdot (\rho \boldsymbol{u}) = 0, \\[4pt] (\rho \boldsymbol{u})_{\overline{t}} + \nabla \cdot (\rho \boldsymbol{u} \otimes \boldsymbol{u} + p \boldsymbol{I}) = 0, \\[4pt] \left(\rho(e + \tfrac{1}{2}\boldsymbol{u}^2) \right)_{\overline{t}} + \nabla \cdot \left(\rho(e + \tfrac{1}{2}\boldsymbol{u}^2)\boldsymbol{u} + p\boldsymbol{u} \right) = 0. \end{array} \right\} \tag{6.1}$$

For simplicity, we assume an ideal gas equation of state,

$$e(p, \rho) = \frac{1}{\gamma - 1} \frac{p}{\rho},$$

where the constant $\gamma > 1$ is the ratio of specific heats. The same analysis applies to general equations of state; the only condition needed is the genuinely nonlinearity of the sound waves. The corresponding sound speed $c(p, \rho) > 0$ is given by

$$c^2 = \frac{\gamma p}{\rho}.$$

There is no flow through the wedge and the solution is even in $\overline{y}$, so that

$$\boldsymbol{u} \cdot \boldsymbol{n} = 0, \tag{6.2}$$

on $\partial \Omega$, where $\boldsymbol{n}$ is the unit normal vector to the boundary $\partial \Omega$. The initial condition

at $\bar{t} = 0$ is

$$
\begin{aligned}
\rho &= \begin{cases} \rho_0, & \bar{x} > 0 \\ \rho_1(\varepsilon), & \bar{x} < 0, \end{cases} \\
\boldsymbol{u} &= \begin{cases} \boldsymbol{0}, & \bar{x} > 0 \\ \boldsymbol{u}_1(\varepsilon), & \bar{x} < 0, \end{cases} \\
p &= \begin{cases} p_0, & \bar{x} > 0 \\ p_1(\varepsilon), & \bar{x} < 0, \end{cases}
\end{aligned} \tag{6.3}
$$

where $(\rho_1, \boldsymbol{u}_1, p_1)$ is the state behind the incident shock, and the small parameter

$$
\varepsilon = \frac{\gamma + 1}{2} \left(\frac{\rho_1 - \rho_0}{\rho_0} \right) \tag{6.4}
$$

measures the shock strength.

Taylor expansion of the Rankine–Hugoniot jump conditions as $\varepsilon \to 0$ implies that ε is given in terms of the incident shock Mach number M by (2.7), to leading order in $M - 1$, and that

$$
\begin{aligned}
\rho_1(\varepsilon) &= \rho_0 \left(1 + \frac{2\varepsilon}{\gamma + 1} \right), \\
\boldsymbol{u}_1(\varepsilon) &= c_0 \left(\frac{2\varepsilon}{\gamma + 1} \boldsymbol{e}_{\bar{x}} + O(\varepsilon^2) \right), \\
p_1(\varepsilon) &= p_0 \left(1 + \frac{2\varepsilon\gamma}{\gamma + 1} + O(\varepsilon^2) \right).
\end{aligned} \tag{6.5}
$$

Here, $\boldsymbol{e}_{\bar{x}}$ is the unit vector in the $\bar{x}$-direction, and $c_0 = c(p_0, \rho_0)$ is the sound speed evaluated at the state ahead of the shock.

7. The linearized solution

The linearized expansion of the solution of (6.1)–(6.3) is

$$
\begin{pmatrix} \rho \\ \boldsymbol{u} \\ p \end{pmatrix} = \begin{pmatrix} \rho_0 \\ \boldsymbol{0} \\ p_0 \end{pmatrix} + \varepsilon \begin{pmatrix} \rho' \\ \boldsymbol{u}' \\ p' \end{pmatrix} (\bar{x}, \bar{y}, \bar{t}) + O(\varepsilon^2). \tag{7.1}
$$

In this limit, the Euler equations (6.1) reduce to the acoustics equations at leading order. The density perturbation ρ' satisfies the wave equation,

$$
\rho'_{\bar{t}\bar{t}} = c_0^2 \Delta \rho'. \tag{7.2}
$$

The other fluid variables can be recovered from ρ' by use of the velocity potential φ, where

$$
\rho' = -\rho_0 c_0^{-2} \varphi_{\bar{t}}, \qquad p' = -\rho_0 \varphi_{\bar{t}}, \qquad \boldsymbol{u}' = \nabla \varphi.
$$

The linearization of the initial conditions (6.3)–(6.5) implies that at $\bar{t} = 0$,

$$
\rho' = \begin{cases} 0, & \bar{x} > 0 \\ 2\rho_0/(\gamma + 1), & \bar{x} < 0. \end{cases} \tag{7.3}
$$

The boundary condition (6.2) implies that

$$
\nabla \rho' \cdot \boldsymbol{n} = 0 \quad \text{on} \quad \partial \Omega. \tag{7.4}
$$

The exact solution of the linearized problem (7.2)–(7.4) was obtained by Keller & Blank (1951). To write out the solution, we introduce similarity variables

$$\left.\begin{array}{c} \bar{\bar{\xi}} = \dfrac{\bar{x}}{c_0\bar{t}}, \quad \bar{\eta} = \dfrac{\bar{y}}{c_0\bar{t}}, \quad \bar{\theta} = \tan^{-1}\left(\dfrac{\bar{y}}{\bar{x}}\right), \\[3mm] \bar{r} = \dfrac{(\bar{x}^2 + \bar{y}^2)^{1/2}}{c_0\bar{t} + (c_0^2\bar{t}^2 - \bar{x}^2 - \bar{y}^2)^{1/2}}, \quad \bar{x}^2 + \bar{y}^2 \leqslant c_0^2\bar{t}^2. \end{array}\right\} \tag{7.5}$$

The incident, reflected, and diffracted wavefronts are located at

$$\left.\begin{array}{ll} \bar{\bar{\xi}} = 1 & \text{(incident)}, \\ \bar{\bar{\xi}} = 1 - \tan 2\theta_w(\bar{\eta} - \tan\theta_w) & \text{(reflected)}, \\ \bar{\bar{\xi}}^2 + \bar{\eta}^2 = 1 & \text{(diffracted)}. \end{array}\right\} \tag{7.6}$$

The region A ahead of the incident discontinuity, the region B behind the incident discontinuity, the region C behind the reflected discontinuity, and the region D occupied by the diffracted wave, are given by

$$\left.\begin{array}{l} A = \left\{(\bar{\bar{\xi}},\bar{\eta}) : \bar{\bar{\xi}} > 1, \quad \theta_w < \bar{\theta} < \pi\right\}, \\[2mm] B = \big\{(\bar{\bar{\xi}},\bar{\eta}) : \bar{\bar{\xi}}^2 + \bar{\eta}^2 > 1 \quad \text{if} \quad 2\theta_w < \bar{\theta} < \pi; \\ \qquad\quad 1 - \tan 2\theta_w(\bar{\eta} - \tan\theta_w) < \bar{\bar{\xi}} < 1 \quad \text{if} \quad \theta_w < \bar{\theta} < 2\theta_w\big\}, \\[2mm] C = \left\{(\bar{\bar{\xi}},\bar{\eta}) : \bar{\bar{\xi}}^2 + \bar{\eta}^2 > 1, \quad \bar{\bar{\xi}} < 1 - \tan 2\theta_w(\bar{\eta} - \tan\theta_w), \quad \theta_w < \bar{\theta} < 2\theta_w\right\}, \\[2mm] D = \left\{(\bar{\bar{\xi}},\bar{\eta}) : \bar{\bar{\xi}}^2 + \bar{\eta}^2 < 1, \quad \theta_w < \bar{\theta} < \pi\right\}. \end{array}\right\} \tag{7.7}$$

The solution is piecewise constant outside the diffracted wavefront,

$$\rho' = \begin{cases} 0, & (\bar{\bar{\xi}},\bar{\eta}) \in A \\ 2\rho_0/(\gamma + 1), & (\bar{\bar{\xi}},\bar{\eta}) \in B \\ 4\rho_0/(\gamma + 1), & (\bar{\bar{\xi}},\bar{\eta}) \in C. \end{cases} \tag{7.8}$$

The solution for $(\bar{\bar{\xi}},\bar{\eta}) \in D$ is given by

$$\rho' = \frac{2\rho_0}{\gamma + 1}\left(1 + \frac{1}{\pi}\tan^{-1}\left[\frac{(1 - \bar{r}^{2\lambda})\cos(\lambda\pi)}{-(1 + \bar{r}^{2\lambda})\sin(\lambda\pi) - 2\bar{r}^\lambda \sin[\lambda(\bar{\theta} - \pi)]}\right]\right.$$
$$\left. + \frac{1}{\pi}\tan^{-1}\left[\frac{-(1 - \bar{r}^{2\lambda})\cos(\lambda\pi)}{(1 + \bar{r}^{2\lambda})\sin(\lambda\pi) - 2\bar{r}^\lambda \sin[\lambda(\bar{\theta} - \pi)]}\right]\right), \tag{7.9}$$

where

$$\lambda = \frac{\pi}{2(\pi - \theta_w)}, \tag{7.10}$$

and the inverse tangent is chosen in the range

$$0 \leqslant \tan^{-1} z \leqslant \pi.$$

The linearized solution is not uniformly valid because its derivatives are infinite at the diffracted wavefront

$$\bar{x}^2 + \bar{y}^2 = c_0^2\bar{t}^2.$$

Nonlinear effects cannot be neglected near the points where this singularity occurs. There are two regions to consider, which we label regions II and III in figure 1.

Region II is a thin region around the point where the diffracted wavefront meets reflected discontinuity in the linearized solution. For small wedge angles, this inner region contains the reflection point where the shock hits the wedge. Region III is a very thin region around the diffracted shock. In region II, both the normal and transverse derivatives of the linearized solution are unbounded. In region III, the derivatives of the linearized solution normal to the wavefront are unbounded.

An inner expansion in region III about the diffracted wavefront can be carried out in a similar way to the analysis in Hunter & Keller (1984). We omit a detailed discussion. The main result is the following expression for the diffracted shock strength as a function of the polar angle $\bar{\theta}$:

$$\frac{[\rho]}{\rho_1} \sim \frac{3}{4} \left(\frac{\gamma+1}{2} \right) \left(\frac{\rho_1 - \rho_0}{\rho_1} \right)^2 \left(\frac{\theta_w}{\pi} \right)^2 \frac{1}{\sin^4 [(\bar{\theta} - \theta_w)/2]}.$$

In the next section, we summarize the inner expansion in region II which leads to the two-dimensional Burgers equation described in §2.

8. The reflection region

In region II, it is convenient to use rotated coordinates aligned with the wedge,

$$\left(\begin{array}{c} \widetilde{x} \\ \widetilde{y} \end{array} \right) = \left(\begin{array}{cc} \cos \theta_w & \sin \theta_w \\ -\sin \theta_w & \cos \theta_w \end{array} \right) \left(\begin{array}{c} \overline{x} \\ \overline{y} \end{array} \right). \tag{8.1}$$

In the rotated coordinated system, the wedge boundary is $\widetilde{y} = 0$ with $\widetilde{x} > 0$, and the linearized location of the reflection point is

$$\widetilde{x} = c_0 (\sec \theta_w)\widetilde{t}, \qquad \widetilde{y} = 0,$$

where $\widetilde{t} = \bar{t}$.

We look for an asymptotic solution of the Euler equations (6.1) of the form

$$\left(\begin{array}{c} \rho \\ \boldsymbol{u} \\ p \end{array} \right) = \left(\begin{array}{c} \rho_0 \\ \boldsymbol{0} \\ p_0 \end{array} \right) + \varepsilon \left(\begin{array}{c} \rho^{(1)} \\ \boldsymbol{u}^{(1)} \\ p^{(1)} \end{array} \right) (\widehat{x}, \widehat{y}, \widehat{t}) + \varepsilon^{3/2} \left(\begin{array}{c} \rho^{(2)} \\ \boldsymbol{u}^{(2)} \\ p^{(2)} \end{array} \right) (\widehat{x}, \widehat{y}, \widehat{t}) + O(\varepsilon^2), \tag{8.2}$$

where the inner variables $(\widehat{x}, \widehat{y}, \widehat{t})$ are defined by

$$\widehat{x} = \frac{\widetilde{x} - c_0\widetilde{t}}{\varepsilon}, \qquad \widehat{y} = \frac{\widetilde{y}}{\varepsilon^{1/2}}, \qquad \widehat{t} = \widetilde{t}. \tag{8.3}$$

We use (8.2)–(8.3) in the Euler equations (6.1), expand the result in powers of $\varepsilon^{1/2}$, and equate coefficients of powers of $\varepsilon^{1/2}$ to zero. This gives

$$\left(\begin{array}{c} \rho^{(1)} \\ \boldsymbol{u}^{(1)} \\ p^{(1)} \end{array} \right) = \widehat{u}(\widehat{x}, \widehat{y}, \widehat{t}) \left(\begin{array}{c} \rho_0 \\ c_0 \boldsymbol{e}_{\widetilde{x}} \\ \gamma p_0 \end{array} \right), \qquad \left(\begin{array}{c} \rho^{(2)} \\ \boldsymbol{u}^{(2)} \\ p^{(2)} \end{array} \right) = \widehat{v}(\widehat{x}, \widehat{y}, \widehat{t}) \left(\begin{array}{c} 0 \\ c_0 \boldsymbol{e}_{\widetilde{y}} \\ 0 \end{array} \right), \tag{8.4}$$

where the vector $\boldsymbol{e}_{\widetilde{x}}$ is the unit tangent vector to the wedge and $\boldsymbol{e}_{\widetilde{y}}$ is the unit normal vector to the wedge. Thus, $\widehat{u}$ is a scaled $\widetilde{x}$-component of velocity, and $\widehat{v}$ is a scaled $\widetilde{y}$-component of velocity. The density and pressure perturbations are proportional to $\widehat{u}$. The flow is irrotational and isentropic up to small corrections of the order ε^3 which

do not influence the leading-order solution. The functions $\widehat{u}$ and $\widehat{v}$ satisfy

$$\left.\begin{array}{l} \widehat{u}_{\widehat{t}} + \left(\dfrac{\gamma+1}{4}c_0\widehat{u}^2\right)_{\widehat{x}} + \tfrac{1}{2}c_0\widehat{v}_{\widehat{y}} = 0, \\[2mm] \widehat{v}_{\widehat{x}} - \widehat{u}_{\widehat{y}} = 0. \end{array}\right\} \tag{8.5}$$

The introduction of normalized asymptotic variables,

$$u = \frac{\gamma+1}{2}\widehat{u}, \qquad v = \frac{\gamma+1}{2\sqrt{2}}\widehat{v}, \qquad x = \widehat{x}, \qquad y = \sqrt{2}\widehat{y}, \qquad t = c_0\widehat{t}, \tag{8.6}$$

reduces (8.5) to (2.5). From (8.2)–(8.4) and (8.6), the physical variables are given in terms of the normalized asymptotic variables by (2.6) and (2.8).

9. Matching

We obtain initial conditions for the two-dimensional Burgers equation (8.5) by matching the inner, weakly nonlinear solution with the outer, linearized solution given in §7. The matching procedure leads to far-field conditions, but far-field conditions are equivalent to initial conditions because the problem is self-similar.

As shown in figure 1, the linearized solution breaks down in the small region II near $(\widetilde{x},\widetilde{y}) = (c_0 t, 0)$. In this region, the leading-order approximation is provided by the weakly nonlinear solution. Since $\theta_w = O(\varepsilon^{1/2})$, we write

$$\theta_w = \varepsilon^{1/2}\widehat{a}, \tag{9.1}$$

where $\widehat{a}$ is an order-one parameter. From (8.3), the outer limit of the inner solution is given by the limit $|(\widehat{x},\widehat{y})| \to \infty$. The inner limit of the outer solution, $\widehat{\lim}$, is given by

$$\widehat{\lim_{\varepsilon\to 0}} \quad \Rightarrow \quad \varepsilon \to 0 \text{ with } \widehat{x}, \widehat{y}, \widehat{t}, \widehat{a} \text{ fixed.}$$

From (8.1)–(8.4) and (7.1) the matching condition is that

$$\widehat{u} \sim \widehat{u}' \quad \text{as} \quad |(\widehat{x},\widehat{y})| \to \infty, \tag{9.2}$$

where

$$\widehat{u}' = \widehat{\lim_{\varepsilon\to 0}} \left(\frac{\rho'}{\rho_0}\right). \tag{9.3}$$

Since the problem for $\widehat{u}$ is self-similar, the matching condition (9.2) is equivalent to an initial condition

$$\widehat{u} \sim \widehat{u}', \quad \text{as} \quad \widehat{t} \to 0^+. \tag{9.4}$$

To compute the matching data $\widehat{u}'$ in (9.3) we introduce asymptotic similarity variables,

$$\widehat{\xi} = \frac{\widehat{x}}{c_0\widehat{t}}, \qquad \widehat{\eta} = \frac{\widehat{y}}{c_0\widehat{t}}, \qquad \widehat{r}^2 = -(2\widehat{\xi} + \widehat{\eta}^2). \tag{9.5}$$

From (7.5), (8.1), (8.3), and (9.1), we find that in the inner limit

$$\left.\begin{array}{l} \overline{\xi} = 1 + \varepsilon(\widehat{\xi} - \widehat{a}\widehat{\eta} - \tfrac{1}{2}\widehat{a}^2) + O(\varepsilon^2), \\[2mm] \overline{\eta} = \varepsilon^{1/2}(\widehat{\eta} + \widehat{a}) + O(\varepsilon^{3/2}). \end{array}\right\} \tag{9.6}$$

From (7.1), (9.1), and (9.5), the inner limits of the shock locations are

$$\left.\begin{array}{ll} \widehat{\xi} = \widehat{a}\widehat{\eta} + \tfrac{1}{2}\widehat{a}^2 & \text{(incident),} \\ \widehat{\xi} = -\widehat{a}\widehat{\eta} + \tfrac{1}{2}\widehat{a}^2 & \text{(reflected),} \\ \widehat{\xi} = -\tfrac{1}{2}\widehat{\eta}^2 & \text{(diffracted).} \end{array}\right\} \tag{9.7}$$

Thus, the circular diffracted wavefront is mapped to a parabola.

Use of these expressions in (7.8), (7.9), and (9.3) implies that the matching data $\widehat{u}'$ is given by

$$\widehat{u}' = \begin{cases} 0 & \text{ahead of the incident shock} \\ 2/(\gamma + 1) & \text{behind the incident shock} \\ 4/(\gamma + 1) & \text{behind the reflected shock,} \end{cases} \tag{9.8}$$

and, inside the diffracted wave, by

$$\widehat{u}' = \frac{2}{\gamma + 1} \left\{ 1 + \frac{1}{\pi} \tan^{-1} \left[\frac{2\widehat{a}\widehat{r}}{\widehat{r}^2 + \widehat{\eta}^2 - \widehat{a}^2} \right] \right\}.$$

This matching data is the exact solution of the reflection problem for the linearized two-dimensional Burgers equation.

As $\widehat{t} \to 0^+$, the parabolic diffracted wavefront and the reflected shock collapse to the half-line $\widehat{y} = 0$, $\widehat{x} \leqslant 0$. Use of (9.5), (9.7) and (9.8) in the matching condition (9.4) implies that

$$\widehat{u} \sim \begin{cases} 0, & \widehat{x} > \widehat{a}\widehat{y} \\ 2/(\gamma + 1), & \widehat{x} < \widehat{a}\widehat{y} \end{cases} \qquad \text{as } \widehat{t} \to 0^+,$$

in $\widehat{y} > 0$. Writing this condition in terms of the normalized asymptotic variables (8.6) and a normalized wedge angle,

$$a = \frac{\widehat{a}}{\sqrt{2}}, \tag{9.9}$$

we get the initial condition stated in (2.9). The expression for a in (2.4) follows from (2.7), (9.1), and (9.9).

REFERENCES

BALLHAUS, W. F. & LOMAX, H. 1975 The numerical simulation of low frequency unsteady transonic flow fields. *Proc. 4th Intl Conf. on Numerical Methods in Fluid Mechanics* (ed. R. D. Richtmyer). Lecture Notes in Physics, vol. 35, pp. 57–63.

BEN-DOR, G. & GLASS, I. I. 1979 Domains and boundaries of non-stationary oblique shock-wave reflexions. Part 1. Diatomic gas. *J. Fluid Mech.* **92**, 459–496.

BLEAKNEY, W. & TAUB, A. H. 1949 Interaction of shock waves. *Rev. Mod. Phys.* **21**, 584–605.

BRIO, M. & HUNTER, J. K. 1992 Mach reflection for the two-dimensional Burgers equation. *Physica D* **60**, 194–207.

BRIO, M. & HUNTER, J. K. 1994 A von Neumann reflection for the 2-D Burgers equation. *Proc. Symp. Appl. Maths* **48**, 265–268.

BRIO, M. & HUNTER, J. K. 1995 Irregular reflection of weak shocks. In *Proc. 5th Intl Conf. on Hyperbolic Problems* (ed. J. Glimm *et al.*), pp. 347–353. World Scientific.

BRIO, M., ZAKHARIAN, A. R., HUNTER, J. K. & WEBB, G. 2000 The von Neumann paradox in weak shock reflection. Submitted to *J. Fluid Mech.*

ČANIĆ, S. & KEYFITZ, B. L. 1998 Riemann problems for the two-dimensional unsteady transonic small disturbance equation. *SIAM J. Appl. Maths* **58**, 1365–1393.

ČANIĆ, S. & MIRKOVIĆ, D. 1998 A numerical study of Riemann problems for the two-dimensional unsteady transonic small disturbance equation. *SIAM J. Appl. Maths* **58**, 1365–1393.

COLE, J. D. & COOK, L. P. 1986 *Transonic Aerodynamics*. Elsevier.

COLE, J. D., COOK, L. P. & SCHLEINIGER, G. 1997 Unsteady transonic flow: Flow about a suddenly deflected wedge. *AIAA J.* **35**, 1179-1186.

COLELLA, P. & HENDERSON, L. F. 1990 The von Neumann paradox for the diffraction of weak shock waves. *J. Fluid Mech.* **213**, 71–94.

COURANT, R. & FRIEDRICHS, K. O. 1976 *Supersonic Flow and Shock Waves*. Springer.

ENQUIST, B. & MAJDA, A. 1981 Numerical radiation boundary conditions for unsteady transonic flow. *J. Comput. Phys.* **40**, 91–103.

GAMBA, I., ROSALES, R. R. & TABAK, E. 1999 Constraints on the formation of singularities for the transonic small disturbance equations. *Commun. Pure Appl. Maths* **52**, 763–779.

GUDERLEY, K. G. 1962 *The Theory of Transonic Flow*. Pergamon.

HENDERSON, L. F. 1966 On a class of multi-shock intersections in a perfect gas. *Aero. Q.* **17**, 1–20.

HENDERSON, L. F. 1987 Regions and boundaries for diffracting shock wave systems. *Z. Angew. Math. Mech.* **67**, 73–86.

HENDERSON, L. F. & MENIKOFF, R. 1998 Triple-shock entropy theorem and its consequences. *J. Fluid Mech.* **366**, 179–210.

HUNTER, J. K. 1991 Nonlinear geometrical optics. In *Multidimensional Hyperbolic Problems and Computations*. IMA Volumes in Mathematics and its Applications, Vol. 29 (ed. A. J. Majda & J. Glimm), pp. 179–197. Springer.

HUNTER, J. K. & KELLER, J. B. 1984 Weak shock diffraction. *Wave Motion* **6**, 79–89.

KELLER, J. B. & BLANK, A. 1951 Diffraction and reflection of pulses by wedges and corners. *Commun. Pure Appl. Maths* **4**, 75–94.

LIGHTHILL, M. J. 1949 The diffraction of a blast. I. *Proc. R. Soc. Lond.* A **198**, 454–470.

MORAWETZ, C. S. 1956a On the nonexistence of continuous transonic flows past profiles, I. *Commun. Pure Appl. Maths* **9**, 45–68.

MORAWETZ, C. S. 1956b On the nonexistence of continuous transonic flows past profiles, II. *Commun. Pure Appl. Maths* **10**, 107–131.

MORAWETZ, C. S. 1956c On the nonexistence of continuous transonic flows past profiles, III. *Commun. Pure Appl. Maths* **11**, 129–144.

MORAWETZ, C. S. 1982 The mathematical approach to the sonic barrier. *Bull. Am. Math. Soc.* **6**, 127–145.

MORAWETZ, C. S. 1994 Potential theory for regular and Mach reflection of a shock at a wedge. *Commun. Pure Appl. Maths* **47**, 593–624.

NEUMANN, J. VON 1963 *Collected Works*, Vol 6. Pergamon Press.

PUCKETT, G., HENDERSON, L. F. & COLELLA, P. 1995 A general theory of anomalous shock refraction. In *Shock Waves @ Marseille IV* (ed. R. Brun & L. Z. Dumitrescu), pp. 139–144. Springer.

RICHTMEYER, R. D. 1981 *Principles of Mathematical Physics*, Vol. I. Springer.

SAKURAI, A. 1964 On the problem of weak Mach reflection. *J. Phys. Soc. Japan* **19**, 1440–1450.

SASOH, A., TAKAYAMA, K. & SAITO, T. 1992 A weak shock wave reflection over wedges. *Shock Waves* **2**, 277–281.

STEGER, J. L. & DALSEN, W. R. 1989 Basic numerical methods. In *Unsteady Transonic Aerodynamics* (ed. D. Nixon). Progress in Astronautics and Aeronautics. AIAA.

STERNBERG, J. 1959 Triple-shock-wave intersections. *Phys. Fluids* **2**, 179–206.

TABAK, E. & ROSALES, R. R. 1994 Weak shock focusing and the von Neumann paradox of oblique shock reflection. *Phys. Fluids* **6**, 1874–1892.

TING, L. & LUDLOFF, H. F. 1952 Aerodynamics of blasts. *J. Aero. Sci.* **19**, 317–328.

WHITHAM, G. B. 1974 *Linear and Nonlinear Waves*. John Wiley & Sons.

YANG, H. Q. & PRZEKWAS, A. J. 1992 A comparative study of advanced shock-capturing schemes applied to Burgers' equation. *J. Comput. Phys.* **102**, 139–159.